Investigating Cobalt Corrosion Mechanisms in a Phenazine Producing Bacterium

Annika DeJager,[a] Anna Kirkland,[a*] Aaron Hinz,[b] David R. McMullin,[a] & Daniel S. Grégoire[a#]

[a]Chemistry Department, Carleton University, Ottawa, ON, Canada

[b]Biology Department, Carleton University, Ottawa, ON, Canada

Running Head: Microbially Induced Corrosion of Cobalt

[#]Address correspondence to Daniel S. Grégoire, danielgregoire@cunet.carleton.ca

[*]Present address: Department of Chemistry, University of Toronto, Toronto, ON, Canada

Abstract

Microbially induced corrosion (MIC) costs trillions of dollars yearly by damaging metal infrastructure. MIC occurs when microorganisms oxidize solid elemental metals using redox-active metabolites such as phenazines, which create soluble metal ions. Phenazine-mediated corrosion has been well studied for iron. Whether such pathways can solubilize the economically critical metal cobalt through thermodynamically favourable reactions remains unknown. We hypothesized that Co(0) corrosion by the model bacterium *Pseudomonas chlororaphis* subspecies *aureofaciens* depends on phenazine availability. To test this hypothesis, we compared the corrosion of Co(0) wires and phenazine production over one-week incubations with either wild-type cells or a deletion mutant devoid of the *phz* operon incapable of phenazine biosynthesis. All experiments with live cells were compared to abiotic controls with spent medium, phenazine standards, and sterile medium. Soluble Co(2+) concentrations measured with ICP-MS showed that live cells were essential to cobalt corrosion. The wild-type and Δ*phz* mutant corroded 30-40% of the wire mass [equivalent to ~ 2,500 μM soluble Co(2+)], which was at least 3-fold higher than mass losses for abiotic controls. Both strains decreased wire diameters and produced considerable pitting compared to abiotic controls imaged with SEM-EDX. Cobalt corrosion could be slowed through Co(2+) toxicity and cobalt oxide precipitation. These findings counter studies with iron and biosynthetic gene cluster analyses suggest that corrosion occurred through alternative mechanisms that rely on metal-binding ligand production. This work expands the repertoire of metals solubilized by MIC and shows that MIC can be used for critical metal recovery at the lab scale.

Importance

Microbially induced corrosion costs trillions of dollars yearly by damaging iron-bearing infrastructure but whether it affects the critical metal cobalt is unexplored. This is important to address to better understand the processes that control the environmental fate cobalt and leverage biological corrosion towards metal reclamation. This study uses the model *Pseudomonas chlororaphis* subspecies *aureofaciens* to test if the production of widely produced redox active phenazines metabolites can corrode elemental cobalt. We repeatedly observed cells corrode cobalt even in the absence of phenazines. We showed that cobalt toxicity and precipitation of cobalt oxides limited corrosion through mechanisms that will be characterized in future work. This study underscores the need to consider corrosion mechanisms beyond those reported for iron. Confirming these mechanisms will be critical to optimizing sustainable recovery strategies that rely on microbially induced corrosion to recover cobalt from electronic waste, which is a global pollution issue.

Introduction

Microbially-induced corrosion (MIC) due to biofilm formation is estimated to damage metal-bearing infrastructure at a cost on the order of trillions of USD per year (1-5). MIC occurs when bacteria or archaea oxidize solid elemental metals into soluble ions (1). Diverse metabolic guilds that thrive along the redox gradients within biofilms contribute to MIC (1). These guilds include anaerobic heterotrophic bacteria, nitrate-reducing bacteria, iron-reducing bacteria, sulphate-reducing bacteria, acetogenic bacteria, and methanogenic archaea (1,6).

MIC mechanisms described in model organisms from these guilds rely on direct electron transfer (DET) or mediated electron transfer (MET) between cells and metal surfaces (6-8). Multiple species are capable of corroding metals through both types of pathways depending on growth conditions and reaction kinetics (1,9-12). DET has been observed in model iron-reducing bacteria and methanogenic archaea that couple Fe(0) oxidation to energy production through direct contact between metals and multi-heme outer surface *c*-cytochromes or electroconductive pili (8-14). MET can be facilitated by hydrogenase-mediated H_2 oxidation or organic acid deprotonation, which produce protons that can accept electrons from metal surfaces, promote corrosion, and regenerate H_2 (1,15-21). MET can also occur when redox-active metabolites (*e.g.,* flavins and phenazines) oxidize metals (1,22-30), given their capacity to act as exogenous electron acceptors that typically shuttle electrons in and out of cells to maintain redox balance (31,32).

The current mechanistic understanding of MIC primarily stems from studies on iron and stainless steel (1,2,6-8). Although the focus on iron-based materials is understandable given concerns surrounding damage to infrastructure, MIC mechanisms that affect the chemistry of other metals remain understudied. MIC has the potential to mobilize elemental metals into nearby environments through oxidation, given evidence that MET within biofilms accelerates the corrosion of non-ferrous metals (33-44). Previous work has demonstrated that MIC of Al(0) alloys occurs through H_2 and organic acid-mediated MET pathways (33-35). H_2S, oxalic acid, and NH_3 have all been linked to the MIC of Cu(0) (36-38). Riboflavin and phenazines have also been associated with the corrosion of Ni(0) and Ti(0), respectively (39-44).

Despite MET pathways being widespread in metabolically versatile guilds, whether such pathways support the MIC of other economically, environmentally, and physiologically relevant metals remains poorly understood. Uncovering these pathways will advance our understanding of how MIC controls the mobility and toxicity of elemental metals that are prevalent in habitats contaminated with electronic and municipal solid waste (45,46). Assessing if MIC can solubilize metals critical to the global economy could open new possibilities for sustainable metal recovery strategies, reframing MIC as more than an undesirable process that damages infrastructure.

This study tests if phenazines produced by the model bacterium *Pseudomonas chlororaphis* subspecies *aureofaciens* corrode elemental cobalt. We focus on cobalt because it is an essential component of consumer electronics that is a priority for reclaiming from electronic waste because it is mined at great environmental expense (45-47). We selected *P. chlororaphis* subsp. *aureofaciens* because it is a genetically tractable non-pathogenic strain that produces carboxylated and hydroxylated phenazines (48-50). These metabolites are similar to pyocyanin (PYO) and phenazine-1-carboxyamide (PCN) produced by the facultative pathogen *Pseudomonas aeruginosa*, which can corrode Fe, Ti, and Cr by MET (26-30). Lastly, we target phenazine-mediated corrosion because Co(0) oxidation to Co(2+) (E^0_{red} = -0.282 V) by phenazine-1-carboxylic acid (PCA) (E^0_{red} = -0.116 V), the main phenazine produced by *P.*

chlororaphis subsp. *aureofaciens*, is thermodynamically favourable ($\Delta G_0 = -nFE^0_{cell} = -32.04$ kJ/mol) (49-52).

To test this mechanistic hypothesis, we compare the corrosion of Co(0) wires in the presence of wild-type cells to a mutant devoid of the *phz* operon required for phenazine production (31,48). We assess whether PCA can directly corrode Co(0) or if corrosion depends on complex mixtures of other metabolites produced by cells. Multiple independent analytical techniques including ICP-MS, LC-HRMS, and SEM-EDX confirmed that live cells corrode cobalt through pathways that do not rely on phenazines. We propose alternative mechanisms for MIC of cobalt based on biosynthetic gene cluster analyses and consider why our observations run counter to previous work on iron that informed our original hypothesis.

Results & Discussion

Live cells are required for cobalt corrosion, but not phenazines

Live *P. chlororaphis* subsp. *aureofaciens* cells corroded more cobalt than spent and sterile medium treatments after 168-hour incubations. Mean Co(2+) concentrations measured by ICP-MS for the wild-type and Δ*phz* strains increased steadily over 72 hours and plateaued at 2024.82 ± 579.21 μM and 2689.23 ± 434.50 μM, respectively (**Figure 1**). For abiotic treatments, mean Co(2+) concentrations plateaued between 181.90 ± 7.83 μM and 560.32 ± 126.22 μM after 24 hours, which was 4 to 10-fold lower than biotic treatments (**Figure 1**). Statistical comparisons of Co(2+) concentrations at 168 hours confirmed that live cells solubilized significantly ($p < 0.05$) more Co(0) than abiotic treatments (**Figure S1**). No significant difference was observed between wild type and Δ*phz* strains, although the spent medium treatment had significantly higher Co(2+) concentrations compared to sterile medium (**Figure S1**). Medium spiked with the phenazine PCA did not lead to significantly higher corrosion compared to sterile medium, suggesting the metabolite did not corrode Co(0) (**Figure 1** & **Figure S2**).

Cobalt corrosion was confirmed by measuring mass losses from the Co(0) wires to conduct cobalt mass balances and corroborate aqueous Co(2+) measurements. Wires incubated with wild-type and Δ*phz* live cells had mean relative losses of 26.22 ± 12.02% and 34.11 ± 2.65% of their starting mass, which were 3 to 10-fold greater than the relative losses recorded for abiotic controls (**Table S1**). Mean cobalt recoveries for all experiments ranged from 99.01 ± 1.35 % and 125.45 ± 3.57% with an average of 102.32 ± 11.56%, indicating that all cobalt in the system was accounted for (**Table S1**). Only the Δ*phz* experiments deviated from the target of 100%. Evapoconcentration is unlikely to be the cause of this discrepancy because water mass balances were in line with expectations (~92 to 97%), suggesting analytical variance in this treatment is a contributing factor (**Table S1**). We verified whether correcting for recoveries affected Co(2+) comparisons at 168 hours and our statistical conclusion did not change (**Figure S1B**).

We can confidently rule out that phenazines contribute to cobalt corrosion since the concentrations of Co(2+) recovered from the Δ*phz* treatment are comparable to those of the wild type (**Figure 1**) despite the evident lack of phenazine production by Δ*phz* cells (**Figure 2**). In contrast to Δ*phz* mutants, total phenazine concentrations recovered at 168 hours from representative replicates from wild-type cells and spent medium ranged from 5.33-9.48 μg/mL and 8.69-11.74 μg/mL, respectively (**Figure 2**). PCA was the dominant phenazine, although smaller amounts of 2-OHPCA and 2-OHPHZ were also recorded in these samples (**Figure 2**).

These observations align with previous reports measuring phenazines in this and similar strains, showing that the analytical techniques were appropriate for detecting the absence of phenazines in Δ*phz* mutants (49,50,53,54).

When reconsidering our mechanistic hypothesis, these phenazine measurements suggest that the spent medium treatment should have had higher Co(0) corrosion if MIC depended on the presence of this metabolite, which was not the case (**Figure 1**). Providing PCA at 5-fold higher concentrations than what we recovered from cells did not lead to more corrosion compared to sterile medium (**Figure S2**). Given that spent medium treatment produced significantly more Co(2+) by 168 hours compared to sterile medium and live cells increased corrosion independently of phenazine production, we must refute our initial hypothesis. These results suggest an alternative metabolite or enzymatic reaction controlled by live cells is responsible for corrosion. We consider other potential mechanisms controlling MIC of cobalt further in subsequent sections.

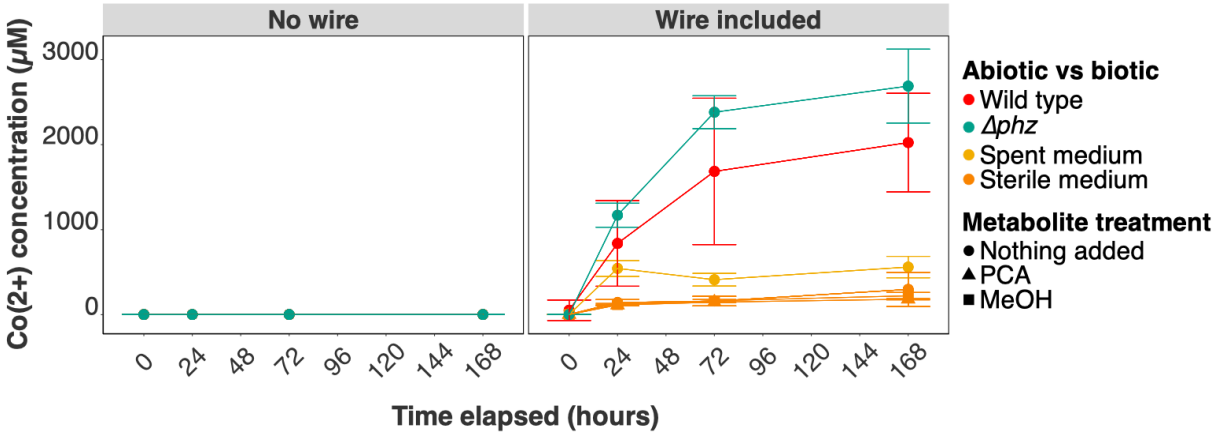

Figure 1: Mean Co(2+) concentrations ± SD obtained by ICP-MS across all biotic and abiotic treatments throughout 168-hour incubations. Wild type: n = 6, Δ*phz*: n = 4, Spent medium: n = 4, and Sterile medium [Nothing added: n = 10, methanol (MeOH) and PCA: n = 3].

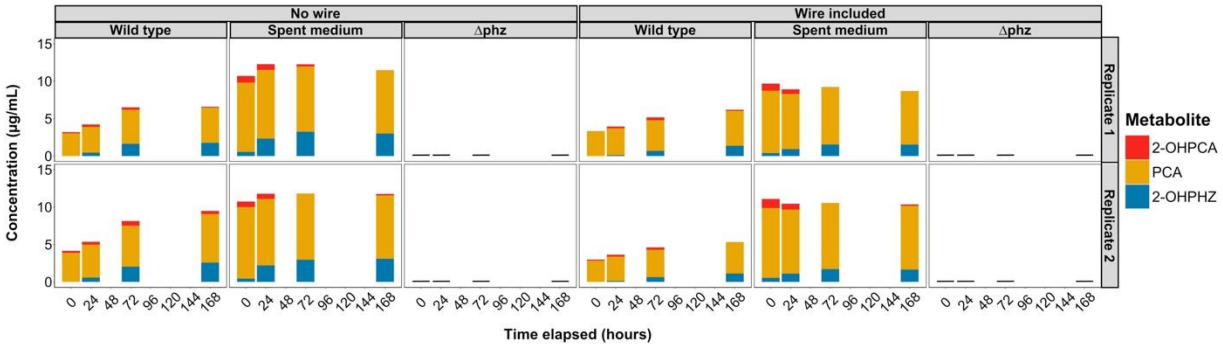

Figure 2: Total phenazine concentration recovered from representative duplicate wild type, Δ*phz*, and spent medium incubations in the presence and absence of Co(0) wires over 168 hours. Stacked bars show contributions of phenazine-1-carboxylic acid (PCA), 2-hydroxyphenazine (2-OHPHZ), and 2-hydroxyphenazine-1-carboxylic acid (2-OHPCA) to the total phenazine amount at each time-point. Black bars are shown in the Δ*phz* to denote that phenazines were not detected at these specific time points.

Cobalt toxicity inhibits corrosion

Having excluded phenazine production as a contributor to cobalt corrosion, we considered how cell viability and Co(2+) uptake could provide additional mechanistic insights on the physiological mechanisms controlling the MIC of cobalt. Viable cell density decreased by orders of magnitude from ~10^8 to ~10^6 CFU/mL during incubation with Co(0) wires, but cells remained viable throughout the entire experiment (**Figure 3**). In contrast, cells from no wire controls showed robust exponential growth, achieving cell densities closer to 10^{10} CFU/mL in stationary phase by 24 hours (**Figure 3**). We suspected that the impaired growth was due to toxic effects of the high concentrations of cobalt solubilized in biotic treatments. Additional tests were conducted to confirm that toxicity stemmed from cells adsorbing and taking up cobalt inside of the cell where we would expect Co(2+) to be most toxic. Comparing samples that had been acidified to lyse cells and release total cobalt content before filtering to samples that had been filtered prior to acidification for ICP-MS analyses showed that 6.64-21.36% (or 77.04-585.63 μM) of Co(2+) was cell-associated (**Figure S3**). This range of concentrations align with dose response experiments, which showed a 50% decrease in growth rate at 23.9 μM Co(2+) (**Figure S4**) and previous reports where 500 μM Co(2+) inhibited the growth of *P. aureofaciens* BS1393 in minimal medium (55).

Although phenazines can help cells manage oxidative stress induced by metal exposure (54,56), the Δ*phz* mutant experienced the same decrease in viability as the wild type cells that maintained phenazine production (**Figure 2** and **Figure 3**). This observation shows phenazine production did not improve tolerance to high μM concentrations of Co(2+). We cannot fully rule out that oxidative stress from cobalt toxicity is managed through other pathways (*e.g.,* glutathione oxidoreductase, super oxide dismutase, or peroxidase), based on genes coding these enzymes being present in the *P. chlororaphis* subspecies *aureofaciens* genome (**Supporting Data 1**). However, these observations also suggest that cobalt toxicity can occur through other mechanisms that are not connected to oxidative stress. These mechanisms may include co-opting uptake pathways required for other essential metals, competition with Fe(2+) binding sites, interactions with thiol-bearing groups on proteins, or indirectly disrupting cell growth by allocating ATP towards an increased need for metal efflux pumps (56-58). Cobalt detoxification mechanisms have been noted for highly-resistant *Geobacter sulfurreducens* (57), while the pathways that confer resistance in this *Pseudomonas* strain require investigation in future work. The toxicity of highly bioavailable ionic metals released immediately by elemental metal oxidation is rarely considered in MIC studies. Our findings highlight the importance of considering toxicity as a potential limitation for MIC in mechanistic studies and *in situ*.

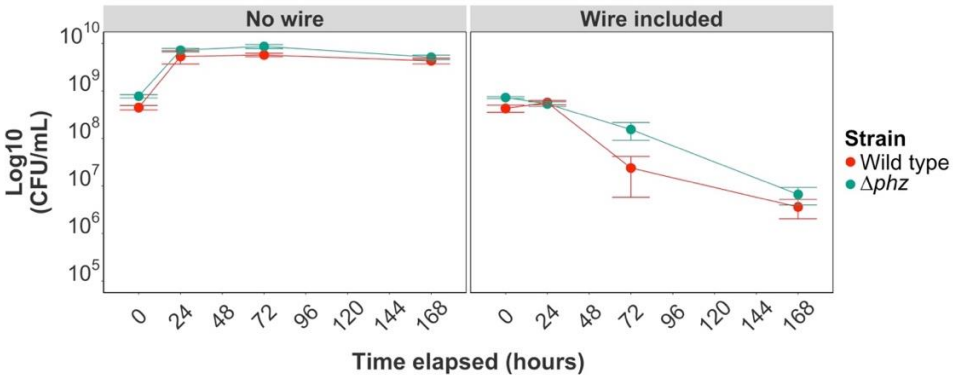

Figure 3: Mean live cell counts of wild type and Δ*phz* cultures in log10(CFU/mL) ± SD over 168-hour corrosion assays. Wild type: n = 6, Δ*phz*: n = 4.

Cobalt oxide precipitation limits pitting from corrosion

Filtering sterile controls prior to acidification revealed greater losses of cobalt (58.9-76.5%, **Figure S5**) relative to the wild type biotic treatment. In this case, we attributed this difference to the abiotic formation of cobalt oxides during storage under normal atmosphere in the absence of cells that produce metabolites that could keep Co(2+) in solution. This observation prompted us to consider how the precipitation of cobalt oxides might hinder MIC through the formation of a passivation layer, as seen in previous MIC studies (1,4,26-29,35,38,43).

We investigated the extent of cobalt precipitation by performing scanning electron microscopy coupled to energy dispersive x-ray (SEM-EDX) analysis on selected representative wires from all treatments (**Figure 4**). The degree of corrosion observed via SEM aligned with the Co(2+) measurements from corrosion assays. Wires in sterile medium showed uniform dissolution of cobalt at the wire surface likely driven by abiotic oxidation but was similar in appearance to the unmanipulated wire (**Figure 4A-C**). Spent medium produced slight changes in wire surface topography and uniform loss of cobalt, as would be expected if more Co(0) was being solubilized by metabolites not present in sterile controls (**Figure 4D** and **Figure S1**). In contrast, wild type and Δ*phz* cells cored out large lengthwise strips on the wires (**Figure 4E,F**). These large areas of corrosion decreased wire diameters by 13.83% and created pits as deep as 60.14 µm (**Figure S5**). Although corrosion patterns varied considerably between live cell replicates based on imaging (**Supporting Data 2**), these observations align with pitting appearance seen in previous MIC studies where *P. aeruginosa* biofilms corroded Fe and Ti stamps (26-30,43,44).

EDX scans of the corroded areas supported that Co(2+) released during abiotic and biotic corrosion formed cobalt oxides at the wire surface in line with the suspected mechanisms of aqueous Co(2+) loss noted for abiotic controls. Scans of representative wires (**Figures S6-S10**) detected Co:O in ratios ranging from ~1:1 to 2:3 based on percent surface weight (**Table S2**). These ratios suggest the possible formation of cobalt(II) oxide (CoO), cobalt(II) hydroxide ($Co(OH)_2$), and cobalt(II/III) oxide (Co_3O_4) formed with cobalt in its respective 2+ and 3+ oxidation states (59). Pink-coloured precipitates were observed in the corrosion flasks, aligning with the formation of cobalt hydroxide in solution with Co(2+) solubilized from the corroding wire. Given the varying ratios of Co:O seen on Co(0) wires across treatments, the exact mechanism contributing to cobalt oxide formation remains unclear.

In earlier iterations of this work, we attempted to solubilize phenazines in DMSO before moving to methanol as a more compatible solvent for LC-HRMS analysis. These early

experiments serendipitously allowed us to revisit the impact of oxide formation on the MIC of cobalt. The addition of DMSO inadvertently led to the formation of large crystalline oxides on the wire surface that increased the diameter of the wire by ~10% (**Figure S11**). DMSO addition significantly decreased Co(2+) concentrations recovered at 168 hours in the presence of live wild-type cells (**Figure S12**). These observations further suggest that the formation of cobalt oxides can preclude cells and/or their metabolites accessing Co(0), which is essential to MIC of cobalt.

The formation of passivation layers is a plausible explanation for why abiotic Co(2+) production plateaus after 24 hours as a protective layer of cobalt oxides forms following abiotic oxidation (**Figure 1** and **Figures S6-S8**). Live cells likely limit the formation of the passivation layer by actively taking up Co(2+) and producing metabolites that form stable complexes with Co(2+). These two processes could limit the abiotic oxidation of cobalt ions by slowing the rate of CoO precipitation in live cell-treated wires to ensure that Co(0) remains accessible for MIC.

This explanation is supported by earlier experiments we conducted using beta-mercaptoethanol as a ligand to form a coloured complex with Co(2+) that could be quantified via spectrophotometry (57) (**Supporting Methods**). These colorimetric methods reliably detected Co(2+) in standards made with $CoCl_2$, but did not align with the high μM concentrations of Co(2+) in live cell experiments that were cross-validated with ICP-MS (**Figure S13A**). We performed additional experiments providing cystine as a biologically relevant metal-binding ligand in equimolar amounts to beta-mercaptoethanol, which eliminated our capacity to detect Co(2+) in $CoCl_2$ standards (**Figure S13B**). These results reinforce that cells are producing ligands that interact with Co(2+) during or following MIC. The exact nature of these ligands and their capacity to inhibit passivation require formal characterization in future work.

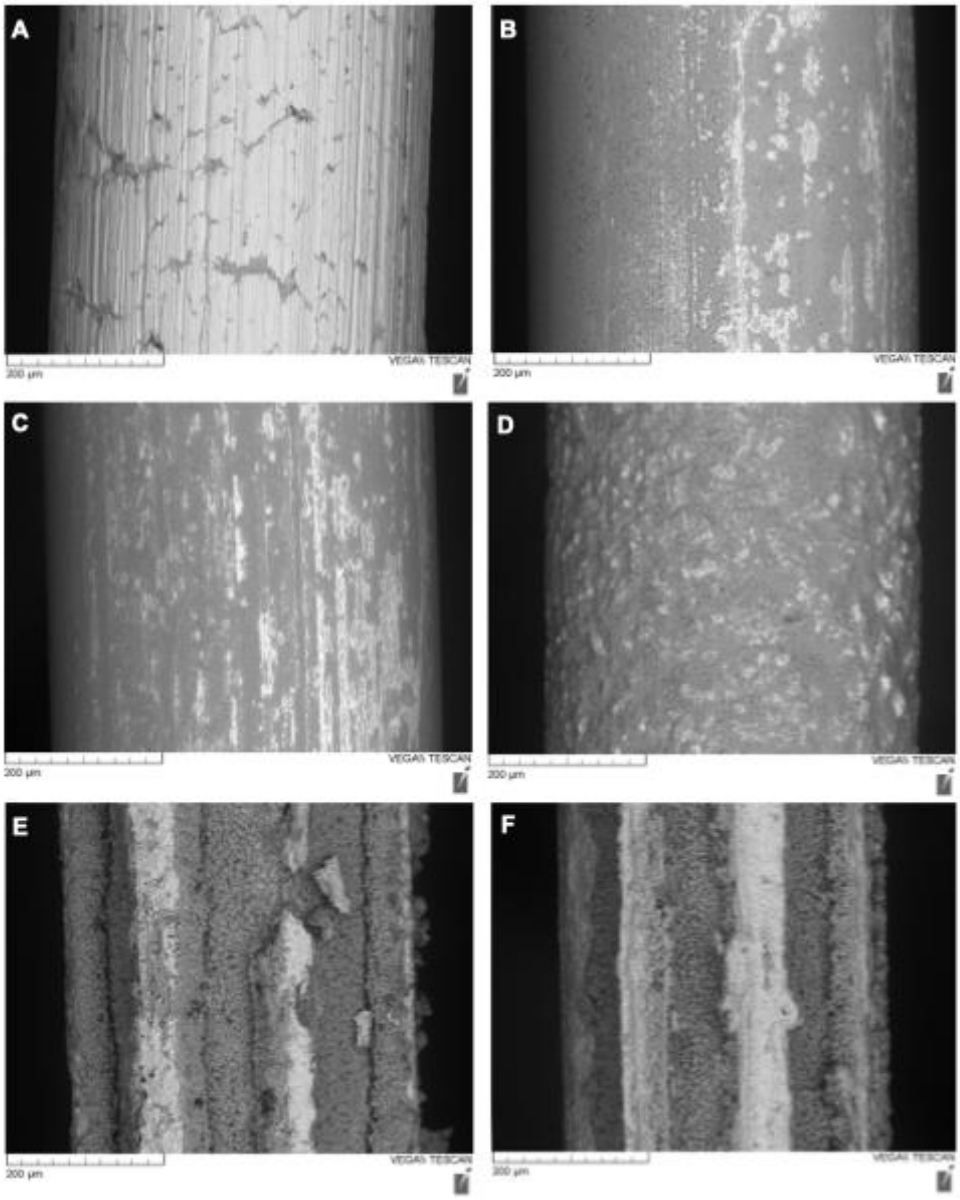

Figure 4: SEM images of Co(0) wires across all treatments after 168 hours of corrosion. Wires were magnified to 400X and images obtained using the back scatter electron detector are displayed. A) Untreated wire. B) Sterile medium. C) PCA. D) Spent medium. E) Wild type. F) Δ*phz*.

Alternative mechanisms for cobalt corrosion

We carried out functional analyses of the *P. chlororaphis* subsp. *aureofaciens* genome to identify other pathways that could potentially contribute to MIC of cobalt. Genome annotations showed one hit to KEGG ID K19640, coding the two-component system protein, hydrogenase maturation factor HypX/HoxX (**Supporting Data 1**). This protein is required for functional hydrogenase complexes in other bacteria and pseudomonads (60,61). However, no other *hup*, *hyb*, or *hox* genes required for hydrogen uptake and oxidation were detected (62), the latter of which has been linked to iron cycling by *Geobacter sulfurreducens* (8,63) (**Supporting Data 1**). Multiple genes associated with cytochrome c-oxidases were also annotated, however no

homologs to the *omc* genes associated with DET in past MIC studies were detected (7-9,11,13). Some cytochromes have a critical role in central redox metabolism and most of the genes we annotated are needed for functioning cytochrome c-oxidases to support respiration. Additional genes coding cobalt uptake/efflux (*i.e.*, KEGG IDs K03699 & K16264) and cobalamin synthesis pathways were detected (*e.g.,* cobaltochelatase encoded by *cobN*) (64,65) (**Supporting Data 1**). These genes could facilitate MIC by favouring intracellular Co(2+) uptake and limiting cobalt oxide formation.

Biosynthetic gene cluster annotations provide explanations that better align with the differences observed in corrosion assays. Annotations with antiSMASH showed that *P. chlororaphis* subsp. *aureofaciens* carries the *hcn* genes required for cyanide production in regions 2 and 7 (**Figure 5** and **Table S3**). Biogenic cyanide production has been associated with gold, platinum, and cobalt solubilization (66-68). Whether this pathway is contributing to cobalt solubilization is questionable because biogenic cyanide production relies on supplying cells with glycine as a carbon and nitrogen source (67). Although we did not supply glycine to cells, DRAM annotations for region 7 detected genes coding for a sarcosine (*N*-methyl glycine) oxidase subunit that could supply glycine via amino acid metabolism (69) (**Table S3**). We did not monitor cyanide production based on our initial mechanistic hypothesis so we cannot fully discount that biogenic cyanide production facilitates the MIC of Co(0) by acting as a ligand for Co(2+).

Region 6 identified by antiSMASH is predicted to produce siderophores via a non-ribosomal peptide (NRP) synthase (**Figure 5**). The core biosynthetic genes in region 6 showed 46 to 53% similarity to genes involved in the production of schizokinen and vibrioferrin (chemical structures provided in **Table S4**). Schizokinen is a known siderophore produced by cyanobacteria (70) and bacteria (71), while vibrioferrin plays a similar role in iron acquisition by *Vibrio alginolyticus* (72). These same genes were identified as coding proteins that produced staphyloferrin, a siderophore identified in members of the *Staphylococcus* genus (73) (**Table S3**). These observation suggest that additional metallophores involved in metal scavenging could be contributing to MIC of cobalt by binding to Co(2+).

Similarly, regions 10 and 11 identified by antiSMASH are predicted to produce a NRP synthetase (NRPS) and metallophore similar to Pf-5 pyoverdine. Pyoverdines are well-characterized metabolites involved in metal uptake in *P. aerugi*nosa and are known to form complexes with cobalt (74,75). In the case of region 11, the second-best hit to this large NRPS was for a siderophore called azotobactin-D isolated from *Azotobacter vinelandii* strain D similar to pyoverdine SXM-1 (76) (**Table S4**). The genes involved in the production of these putative metabolites occur alongside genes involved in siderophore transport inside of the cell (**Table S3)**. This observation further suggests that uptake of Co(2+) bound to metallophores is important to consider in the context of the physiological mechanisms that can control the MIC of cobalt.

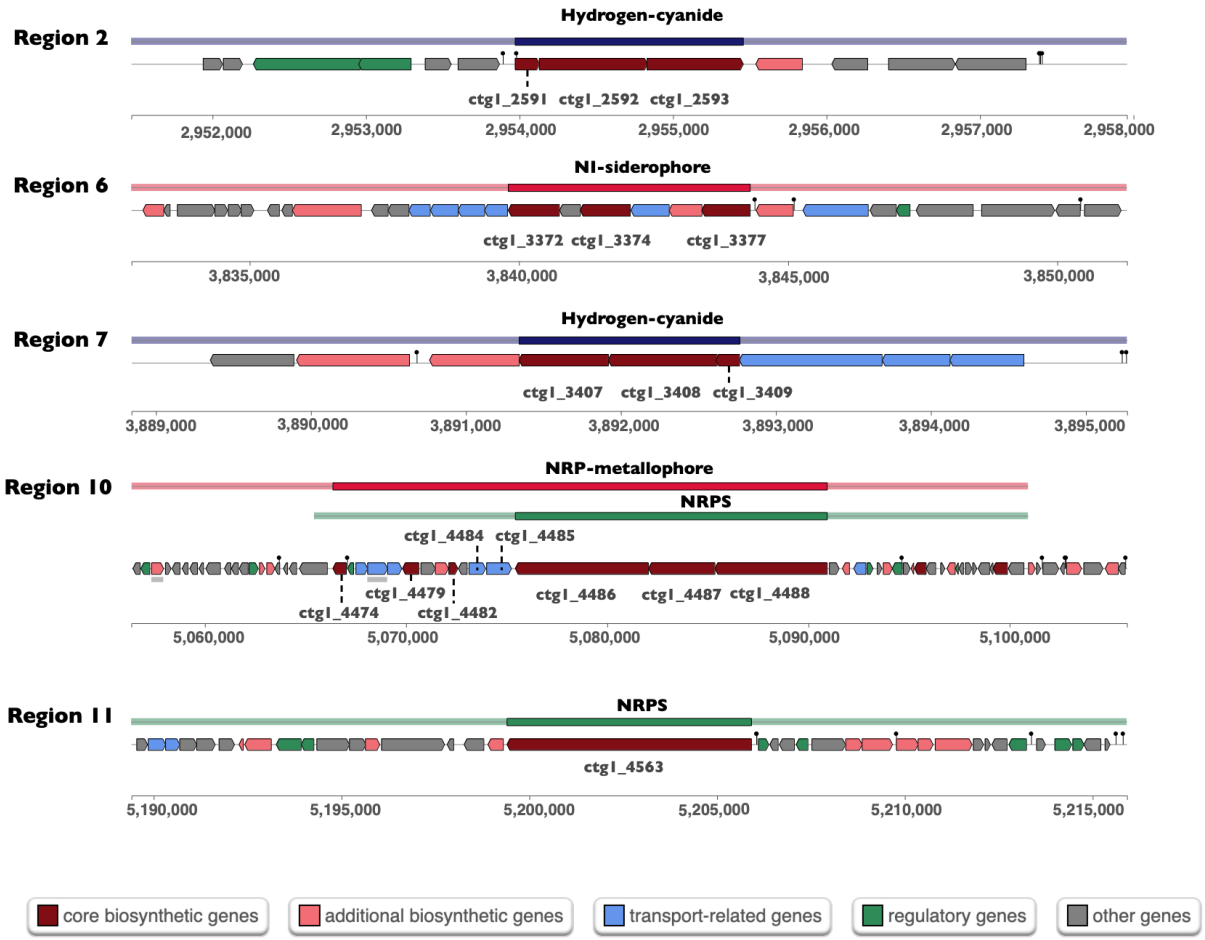

Figure 5: Summary of antiSMASH output with the "strict" setting for biosynthetic gene clusters predicted to produce metabolites relevant to cobalt solubilization and transport. Visualizations were exported and manually edited in image editing software to add antiSMASH loci indicators for core biosynthetic genes and select transport-related genes that were independently annotated using KEGG and Uniref90 databases via DRAM (shown in **Table S3**). Hashed lines were added to clearly link identifiers to smaller genes in the biosynthetic gene clusters for clarity.

Conclusion

Our study provides multiple independent tests that show *P. chlororaphis* subsp. *aureofaciens* can corrode elemental cobalt. We demonstrate that cobalt corrosion relies on the presence of actively growing cells that produce metabolites other than phenazines. We highlight that cobalt toxicity and the precipitation of cobalt oxides are key processes that can limit MIC. We identify alternative pathways for MIC that rely on metal-binding ligands that warrant further mechanistic study.

These findings contradict thermodynamic predictions that suggest phenazine-mediated Co(0) oxidation would still be thermodynamically favourable with the phenazine and Co(2+) concentrations used in the PCA treatments in this study (ΔG = -37.07 kJ/mol) (**Table S5**). Furthermore, these findings do not align with previous work where *phz* gene deletions eliminated the capacity for *P. aeruginosa* to corrode metal surfaces (26-30,43). One potential explanation

for this disparity is that phenazines excreted by the cell were in their reduced state and couldn't act as oxidants. Alternatively, phenazine-mediated corrosion may have unforeseen kinetic limitations that limited the rate at which oxygen could replenish the pool of oxidized phenazines with and without cells. It is also possible that previous *phz* gene deletions in *P. chlororaphis* subsp. *aureofaciens* and the best studied model *P. aeruginosa* led to different regulatory network disruptions with unforeseen impacts on metallophore production that could affect net MIC. Regardless of why phenazines did not corrode cobalt, our work highlights the need to consider alternative mechanistic hypothesis for cell-derived ligands and metallophores in future MIC work. We plan to test alternative hypothesis in future work by using RNA sequencing to guide gene deletions efforts using the approaches we optimized for *P. chlororaphis* subsp. *aureofaciens*.

Identifying these mechanisms will be critical to expanding MIC studies beyond iron to understand the environmental fate of critical metals and leverage MIC for sustainable metal recovery. Elemental metals including cobalt are prevalent at mg/kg concentrations in electronic waste streams, underscoring the need for sustainable metal reclamation strategies to mitigate the negative impacts of this global waste stream. MIC-based strategies that rely on naturally occurring metabolites produced under mesophilic and circumneutral conditions offer an ideal way to circumvent the large environmental footprints associated with pyrometallurgical and hydrometallurgical metal extraction methods that are the current standard (77,78). Although MIC is a major concern when it comes to damaging infrastructure, we make the case for shifting the narrative on MIC to consider opportunities for sustainable metal reclamation starting with cobalt.

Methods

Bacterial Strains and Culture Conditions

All corrosion assays were conducted using bacterium *Pseudomonas chlororaphis* subspecies *aureofaciens* (ATCC 13985), originally isolated from kerosene-contaminated clay of the Maas River. Cells were grown aerobically at 28 ˚C and shaken at 220 rpm (New Brunswick Scientific Innova® 44) in modified pH 7 Delft mineral salt liquid medium comprised of a basal salt solution, trace metal solution, and glucose solution (55). To prepare the basal solution, 3.88 g K_2HPO_4, 1.63 g NaH_2PO_4, 2.0 g $(NH_4)_2SO_4$ and 0.1 g $MgCl_2{\cdot}6\ H_2O$ were combined in 980 mL of MilliQ water and autoclaved at 121 ˚C for 30 min. For the trace element solution, 100.0 mg EDTA, 20.0 mg $ZnSO_4{\cdot}7\ H_2O$, 10.0 mg $CaCl_2{\cdot}2\ H_2O$, 50.0 mg $FeSO_4{\cdot}7\ H_2O$, 2.0 mg $Na_2MoO_4{\cdot}2\ H_2O$, 2.0 mg $CuSO_4{\cdot}5\ H_2O$, 2.18 mg $CoCl_2$, and 12.2 mg $MnCl_2{\cdot}4\ H_2O$ were dissolved in 100 mL of MilliQ water and filter sterilized using a 0.2 µm PES filter. For the glucose solution, 36.112 g anhydrous D-glucose was dissolved in 100 mL of MilliQ water and filter sterilized using a 0.2 µm PES filter. 10 mL each of these two sterile solutions were added to the basal salt solution after autoclaving. To make solid defined medium, 15 g of agar was added to the basal salt solution prior to autoclaving. The method used to generate a dose-response curve for Co(2+) exposure with *P. chlororaphis* subsp. *aureofaciens* was detailed in **Supporting Methods**.

Construction of Δ*phz* deletion mutant

Deletion mutants were created to remove the entire *phz* operon (*phz*A/B, *phz*C, *phz*D, *phz*E, *phz*F, and *phz*G) from wild-type *P. chlororaphis* subsp. *aureofaciens* using a previously

396 established 2-step allelic exchange method involving antibiotic resistance and sucrose sensitivity
397 markers encoded by the pK18msB gene replacement plasmid (79,80). pK18msB was a gift from
398 Christopher Johnson (Addgene plasmid # 177839; http://n2t.net/addgene:177839; RRID:
399 Addgene 177839). A list of the strains, plasmids, and primers used in the processes detailed
400 below are in Table 1. Additional details on protocols are provided in **Supporting Methods**.
401
402 Table 1: Summary of strains, plasmids, and primers used in genetic manipulations.
403

Strains	**Description/Role**	**Reference/Source**
P. chlororaphis subsp. *aureofaciens* (ATCC 13985)	Wild-type *P. chlororaphis* subsp. *aureofaciens* strain	50, New England Biolabs
P. chlororaphis subsp. *aureofaciens* Δ*phz*10.4	Deletion mutant lacking the *phz* operon, used in corrosion Δ*phz* assays	This study
E. coli NEB5-α pK18msB-Δ*phz*	*E. coli* donor, contains pK18msB harbouring Δ*phz* deletion insert	This study
E. coli HB101 pRK2013 (ATCC 37159)	*E. coli* helper strain, contains pRK2013 with conjugation machinery needed for tri-parental mating	New England Biolabs
Plasmids	**Size & markers**	**Reference**
pK18msB	3.282 kb*, NeoR, KanR, sacB	80, Addgene
pK18msB–Δ*phz*	pK18msB with Δ*phz* deletion allele	This study
pRK2013	48 kb, KanR	81
Primer name	**Sequence (5' to 3')**	**Reference/source**
phz_insert_FW	TCGATCACCGCGTAGTTAGC	This study
phz_insert_RV	CTGGCGATCATGTCCAGGTT	This study

404 *Size observed by gel electrophoresis was approximately 5.7 kb. KanR and sacB markers were
405 validated on the original pK18msB stab culture, so there was no reason to suspect issues with the
406 plasmid in downstream manipulations.
407
408 The deleted sequences spanned from the 31st nucleotide of *phz*A/B to the 639th
409 nucleotide of *phz*G (i.e.: nucleotides 6142474 to 6148700 in wild-type genome). Sequences
410 homologous to 700 bp upstream and 701 bp downstream of the deletion junction were cloned as
411 a 1.4 kb insert onto the pK18msB allelic exchange vector to yield the Δ*phz* deletion plasmid
412 (**Figure S14**). The insert was generated as a synthetic gene fragment (Twist Bioscience), with
413 SacI and XmaI restriction sites added to the ends, and capped by random 6 bp sequence
414 extensions (**Figure S14**). The gene fragment was digested with SacI and XmaI, purified, and
415 ligated to the multiple-cloning site of allelic exchange vector pK18msB using established
416 protocols (79). Validation of fragment sizes and restriction digest efficiency was conducted by
417 agarose gel electrophoresis. Ligation reactions were transformed into *E.coli* NEB5-α chemically
418 competent cells (C2988J, New England Biolabs) with selection on Luria-Bertani (LB) agar
419 amended with 30 µg/mL Kanamycin. KanR colonies were screened by colony PCR with insert-
420 amplifying primers phz_insert_FW and phz_insert_RV to identify transformants carrying the
421 vector successfully ligated to the insert. Successful candidates streaked for isolation on LB + 30

422 µg/mL Kan agar, and verified for sucrose susceptibility (conferred by *sac*B present on
423 pK18msB) on LB + 30 µg/mL Kan agar + 5% sucrose agar.
424 Tri-parental mating was conducted to introduce pK18msB–Δ*phz* from *E. coli* NEB5-α
425 transformants into the recipient *P. chlororaphis* subsp. *aureofaciens* with the help of *E. coli*
426 HB101 harbouring pRK2013, which provided necessary conjugation machinery for this process.
427 The recipient was incubated at 42 ˚C for 1 hour prior to setting up the conjugation reactions to
428 inactivate host-nucleases and a 2:2:1 ratio of donor:helper:recipient cultures was adopted to
429 increase efficiency. Selection protocols detailed are based on those published by Liu et al (82).
430 The first homologous recombination step involving integration of pK18msB–Δ*phz* into the
431 recipient genome was selected for by plating the mating mixture onto LB + 50 µg/mL Kan + 100
432 µg/mL Amp agar. *P. chlororaphis* subsp. *aureofaciens* merodiploid conjugants gain KanR from
433 the pK18msB. The ampicillin counter-selects the *E. coli* donor and helper, while sparing the
434 intrinsically AmpR *P. chlororaphis* subsp. *aureofaciens* cells. Successful conjugants were re-
435 streaked for isolation and then plated on LB + 10% sucrose agar to select for the second
436 recombination step, in which the pK18msB backbone was excised from the recipient genome.
437 Sucrose-resistant candidates were streaked for isolation prior to being screened via
438 colony PCR to distinguish successful deletion mutants possessing the Δ*phz* allele from wild-type
439 revertants (**Figure S15**). Phenotypic validation of loss of KanR, sucrose-sensitivity, and orange
440 colour indicative of phenazine production was performed by streaking on LB alone, LB + 50
441 ug/mL Kan, and LB + 10% sucrose agar (**Figure S16**). *P. chlororaphis* subsp. *aureofaciens*
442 Δ*phz*10.4 was selected as deletion mutant used in cobalt corrosion assays. Comparisons of
443 growth in defined medium showed no notable difference in growth to the wild type (**Figure 1B**).
444
445 <u>Co(0) Corrosion Assays</u>
446
447 Corrosion assays were conducted by incubating 1 cm segments of pure Co(0) wires (0.5 mm
448 diameter, 99%, 010947.BW, Puratonic) in various abiotic or biotic treatments to observe levels of
449 corrosion over 168 hours. Co(0) wires were weighed and sterilized with 30 sec washes in
450 acetone, MilliQ, and ethanol prior to beginning the assays. 'No wire' controls were run in tandem
451 with the wire containing flasks, to distinguish between background Co(2+) in the defined
452 medium and Co(2+) resulting from wire corrosion. Live cell treatments were prepared by
453 growing wild type and Δ*phz* strains in 5 mL of defined medium as previously described. After
454 16-18 hours of growth, inocula were combined with 45 mL of defined medium in 250 mL flasks
455 to make 10% v/v inocula.
456 Abiotic treatments containing phenazine standards and spent medium obtained by
457 vacuum-filtering (0.22 µm pore size PSE filters, 83.3941.001, Sarstedt) 60 mL cultures grown
458 for 24 hours to reach early stationary phase were conducted alongside experiments with live
459 cells. Experiments that provided the main phenazine produced by *P. chlororaphis* subsp.
460 *aureofaciens* used a commercially available phenazine-1-carboxylic acid standard (PCA, 98%,
461 CAS: 2538-68-3, CS-W009046, ChemScene LLC) dissolved in HR-GC grade methanol and
462 spiked to a final concentration of 50 µg/mL. 6.5% v/v methanol only controls were also included
463 to control for the addition of solvent. Prior to settling on methanol as the desired solvent for
464 downstream LC-HRMS, preliminary experiments were run with DMSO as a solvent that are
465 discussed in **Supporting Methods**. Treatments were run alongside 50 mL of sterile medium to
466 observe baseline corrosion caused by the medium devoid of cells, metabolites, and/or other
467 solvents.

Sub-sampling of assay flasks shaken at 28 ˚C and 220 rpm occurred at 0, 24, 72, and 168 hours. Flasks were weighed before and after sub-sampling for water and cobalt mass balance purposes. For each sub-sample, aliquots of 5 mL for LC-HRMS and 2.5-3.5 mL for ICP-MS analyses were transferred to glass vials and polypropylene tubes respectively. 200 µL was taken to measure cell growth by OD_{600} using a BioTek Epoch spectrophotometer. Additionally, plate counts were conducted to assess viability of live cells treatments.

Co(2+) determination by ICP-MS

Sub-sampled volumes for ICP-MS were acidified to 2% v/v with trace element grade HNO_3 (Baker Intra-Analyzed Plus, 9368-01, Avantor) prior to filtering through 0.22 µm hydrophilic PTFE filters. Additional aliquots were taken from duplicate wild type and sterile medium time-series to determine intra-cellular Co(2+) concentrations. These samples were first passed through 0.22 µm hydrophilic PTFE filters to remove cells and then acidified to 2% v/v HNO_3, allowing only the extra-cellular Co(2+) concentration to be detected. All processed samples were then diluted 20-fold prior to ICP-MS analysis. Co(2+) concentrations were determined using two Agilent systems: 7700x ICP-MS with ASX-500 autosampler and 7900x ICP-MS with SPS4 autosampler. Multi-internal standards monitored the recovery of selected elements (7700x ICP-MS = Ge, In; 7900x ICP-MS = Sc, Ge, Y) for quality assurance. Co(2+) standards ranging 0-50 ppm were prepared using VeriSpec® Cobalt Standard for ICP 1000 ppm in 2% HNO_3 (RV010272-100N, Ricca). To ensure consistency between systems, a comparison was conducted with 4 randomly selected time-series across wild type, spent medium, and sterile medium treatments, and showed negligible variance between instruments (~2.57%, **Table S6**). Recovered Co(2+) concentrations were used to conduct a mass balance for cobalt in the system, by comparing aqueous Co(2+) corrected for sub-sampling removals to mass losses on the Co(0) wires. Mean Co(2+) recovery across all treatments was 102.32 ± 11.56% and ranged from 99.01 ± 1.35% to 125.45 ± 3.57% (**Table S1**).

Phenazine quantification by LC-HRMS

5 mL aliquots from duplicate samples of wild type, Δ*phz*, and spent medium time-series were processed using a modified protocol from Liu et al (82). Briefly, samples underwent three freeze-thaw cycles and were then acidified to pH 2 with 110 µL of 3 M HCl before passing through 0.22 µm hydrophilic PTFE filters. Phenazines were extracted with two volumes of ACS grade ethyl acetate and the combined organic layer was evaporated under N_2 and reconstituted in 5 mL of HR-GC grade methanol.

Phenazine (PHE, 99+%, CAS: 92-82-0, A15770.06, Thermo Scientific), 2-OHPHZ (95%, CAS: 4190-95-8, V32899, Ontario Chemicals Inc.), 1-hydroxyphenazine (1-OHPHZ, >95.0%, CAS: 528-71-2, H0289, TCI), and phenazine-1-carboxamide (Oxychlororaphine, 97.46%, CAS: 550-89-0, CS-W022931, ChemScene LLC) standards were sonicated in HR-GC grade methanol until homogenous. These were combined into standards using a 1:1:1:1:1 ratio, where each compound had a final concentration ranging from 0.1 to 7 µg/mL. Extraction efficiency was evaluated by spiking 5 µg/mL of individual phenazine standards into sterile medium. These laboratory fortified solutions underwent extraction and were directly compared to unmanipulated 5-in-1 standards at 5 µg/mL to give mean extraction efficiency values of 81.60 ± 3.85% for 2-OHPHZ, 84.72 ± 1.58% for 1-OHPHZ, 84.59 ± 1.69% for PCA, and 63.99 ± 1.39% for PCN.

LC-HRMS spectra revealing phenazine species present in cell culture extracts were obtained with an Agilent 6230B Time of Flight (ToF) mass spectrometer coupled to an Agilent 1260 Infinity II HPLC system. An Eclipse Plus C18 RRHD column (2.1 × 100mm, 1.8 µm, Agilent Technologies) maintained at 35˚C was used to separate compounds present in 2 µL injections of 5-in-1 standards and experimental samples. The mobile phases consisted of (A) ddH2O with 0.1% formic acid and (B) acetonitrile (ACN) with 0.1% formic acid, with a linear gradient ramping from 5% (B) to 100% (B) over 11 min at a flow rate of 0.4 mL/min. The Agilent 6230B ToF mass spectrometer was operated in ESI positive mode scanning from 100-1700 m/z. Examples of extracted ion chromatograms for phenazines of interest (**Figure S17**) and a summary of retention times, m/z values, and standard curve linearity are provided in Supporting Methods (**Table S7** & **Table S8**). Quantification of 2-OHPCA was conducted using PCA standards as a proxy.

Co(0) wire surface analysis using SEM-EDX

After the 168 hr corrosion assays, Co(0) wires were gently rinsed with deionized water and dried under N_2 before being weighed. Wires were imaged and measured by scanning-electron microscope (SEM, TESCAN VegaII XMU) for evidence of corrosion at 20 kV using backscattered electron (BSE) and low-vacuum secondary electron detectors (LVSTD). Elemental surface composition was analyzed using an energy-dispersive X-ray spectrometer (EDX, Oxford Inca Energy X-Act). Selection of sections for scanning was driven by shading in images indicative of regions high in pure cobalt compared to those of potential passivation layers. All raw images are provided in **Supporting Data 2.**

Bioinformatics analyses

The full genome for *P. chlororaphis* subsp. *aureofaciens* generated using Illumina and Oxford Nanopore long-read sequencing was downloaded from ATCC via this link: https://genomes.atcc.org/genomes/60f7ef6772424c16. Biosynthetic gene clusters and their predicted metabolites were identified by loading the genome directly into the web version of antiSMASH v8.dev-220ad8f9 adjusted to the "strict" setting (83). Specific biosynthetic gene clusters of interest were manually exported as .svg files and edited in graphic software to highlight genetic loci of interest. The genome was also annotated using the Distilled Refined Annotation of Metabolism (DRAM) v.1.5.0 (84) using the KEGG and UniRef90 databases. The annotation file output by DRAM was used to manually search for any gene names containing the strings of text "cobalt", "cob", "cyanide", "cytochrome", "glutathione", "hcn", "hydrogenase", "peroxidase", "siderophore", and "super oxide dismutase" to identify pathways that could be contributing to oxidative stress response and cobalt cycling. Annotations from DRAM were cross-referenced with antiSMASH to confirm putative metabolites and transport pathways potentially involved in the MIC of cobalt. The DRAM annotation file is provided in **Supporting Data 1**.

Statistical analyses

All statistical analyses and data visualizations for ICP-MS, LC-HRMS, and plate counts were carried out using R v 4.3.2 in R studio 2024.09.0+375. Data manipulations and visualizations

were carried using the 'tidyverse' v 2.0.0 and patchwork packages v 1.3.0. Additional details on other statistical analyses are provided where relevant in **Supporting Results.**

Data availability statement

All data underlying main and supporting figures and the associated R notebooks containing code required to reproduce visualizations has been uploaded to the following GitHub page: https://github.com/carleton-envbiotech/Cobalt_corrosion/tree/main. All bash code required for genome annotation workflows has also been provided on the same GitHub page. Finally, all SEM images and summaries of EDX analysis contained in **Supporting Data 2** has been uploaded to Zenodo, and can be accessed using the following link: https://zenodo.org/records/15538446.

Acknowledgements

AD contributed to the conceptualization, methodology, investigation, formal analysis, validation, writing the original draft. AK contributed to the initial conceptualization, methodology, investigation, formal analysis, and validation. AH contributed to the method development and provided resources used for the genetic manipulations. DRM contributed to the LC-HRMS methodology and instrumentation. DSG contributed to the conceptualization, data curation, formal analysis, project administration, resources, software, supervision, reviewing, and editing. All authors contributed to reviewing and editing the manuscript for submission. This work was supported by an NSERC Discovery Grant awarded to DSG (#RGPIN-2022-04891 and DGECR-2022-00512).

References

1. Xu D, Gu T, Lovley DR. 2023. Microbially mediated metal corrosion. Nat Rev Microbiol 21:705–718.
2. Cámara M, Green W, MacPhee CE, Rakowska PD, Raval R, Richardson MC, Slater-Jefferies J, Steventon K, Webb JS. 2022. Economic significance of biofilms: a multidisciplinary and cross-sectoral challenge. npj Biofilms and Microbiomes 8:1–8.
3. Amendola R, Acharjee A. 2022. Microbiologically Influenced Corrosion of Copper and Its Alloys in Anaerobic Aqueous Environments: A Review. Frontiers in Microbiology 13.
4. Wang H, Ju L-K, Castaneda H, Cheng G, Zhang Newby B. 2014. Corrosion of carbon steel C1010 in the presence of iron oxidizing bacteria *Acidithiobacillus ferrooxidans*. Corrosion Science 89:250–257.
5. Booth GH. 1964. Sulphur Bacteria in Relation to Corrosion. Journal of Applied Bacteriology 27:174–181.
6. Gu T, Wang D, Lekbach Y, Xu D. 2021. Extracellular electron transfer in microbial biocorrosion. Current Opinion in Electrochemistry 29:100763.
7. Kracke F, Vassilev I, Krömer JO. 2015. Microbial electron transport and energy conservation – the foundation for optimizing bioelectrochemical systems. Front Microbiol 6:575.
8. Tang H-Y, Holmes DE, Ueki T, Palacios PA, Lovley DR. 2019. Iron Corrosion via Direct Metal-Microbe Electron Transfer. mBio 10:e00303-19.
9. Tang H-Y, Yang C, Ueki T, Pittman CC, Xu D, Woodard TL, Holmes DE, Gu T, Wang F, Lovley DR. 2021. Stainless steel corrosion via direct iron-to-microbe electron transfer by Geobacter species. The ISME Journal 15:3084–3093.
10. Hernández-Santana A, Suflita JM, Nanny MA. 2022. *Shewanella oneidensis* MR-1 accelerates the corrosion of carbon steel using multiple electron transfer mechanisms. International Biodeterioration & Biodegradation 173:105439.
11. Holmes DE, Dang Y, Walker DJF, Lovley DR. 2016. The electrically conductive pili of Geobacter species are a recently evolved feature for extracellular electron transfer. Microbial Genomics 2:e000072.
12. Liang D, Liu X, Woodard TL, Holmes DE, Smith JA, Nevin KP, Feng Y, Lovley DR. 2021. Extracellular Electron Exchange Capabilities of Desulfovibrio ferrophilus and Desulfopila corrodens. Environ Sci Technol 55:16195–16203.
13. Zhou E, Li F, Zhang D, Xu D, Li Z, Jia R, Jin Y, Song H, Li H, Wang Q, Wang J, Li X, Gu T, Homborg AM, Mol JMC, Smith JA, Wang F, Lovley DR. 2022. Direct microbial electron uptake as a mechanism for stainless steel corrosion in aerobic environments. Water Research 219:118553.
14. Holmes DE, Tang H, Woodard T, Liang D, Zhou J, Liu X, Lovley DR. 2022. Cytochrome-mediated direct electron uptake from metallic iron by Methanosarcina acetivorans. mLife 1:443–447.
15. Woodard TL, Ueki T, Lovley DR. H2 Is a Major Intermediate in Desulfovibrio vulgaris Corrosion of Iron. mBio 14:e00076-23.
16. Tsurumaru H, Ito N, Mori K, Wakai S, Uchiyama T, Iino T, Hosoyama A, Ataku H, Nishijima K, Mise M, Shimizu A, Harada T, Horikawa H, Ichikawa N, Sekigawa T, Jinno K, Tanikawa S, Yamazaki J, Sasaki K, Yamazaki S, Fujita N, Harayama S. 2018.

An extracellular [NiFe] hydrogenase mediating iron corrosion is encoded in a genetically unstable genomic island in Methanococcus maripaludis. Sci Rep 8:15149.

17. Lahme S, Mand J, Longwell J, Smith R, Enning D. 2021. Severe Corrosion of Carbon Steel in Oil Field Produced Water Can Be Linked to Methanogenic Archaea Containing a Special Type of [NiFe] Hydrogenase. Applied and Environmental Microbiology 87:e01819-20.
18. Uchiyama T, Ito K, Mori K, Tsurumaru H, Harayama S. 2010. Iron-Corroding Methanogen Isolated from a Crude-Oil Storage Tank. Applied and Environmental Microbiology 76:1783–1788.
19. Jia R, Tan JL, Jin P, Blackwood DJ, Xu D, Gu T. 2018. Effects of biogenic H2S on the microbiologically influenced corrosion of C1018 carbon steel by sulfate reducing *Desulfovibrio vulgaris* biofilm. Corrosion Science 130:1–11.
20. Kato S, Yumotot I, Kamagata Y. 2015. Isolation of Acetogenic Bacteria That Induce Biocorrosion by Utilizing Metallic Iron as the Sole Electron Donor. Applied and Environmental Microbiology 81:67.
21. Davidova IA, Duncan KE, Wiley G, Najar FZ. 2022. Desulfoferrobacter suflitae gen. nov., sp. nov., a novel sulphate-reducing bacterium in the Deltaproteobacteria capable of autotrophic growth with hydrogen or elemental iron. International Journal of Systematic and Evolutionary Microbiology 72:005483.
22. Jin Y, Li J, Zhang M, Zheng B, Xu D, Gu T, Wang F. 2024. Effect of exogenous flavins on the microbial corrosion by *Geobacter sulfurreducens* via iron-to-microbe electron transfer. Journal of Materials Science & Technology 171:129–138.
23. Light SH, Su L, Rivera-Lugo R, Cornejo JA, Louie A, Iavarone AT, Ajo-Franklin CM, Portnoy DA. 2018. A flavin-based extracellular electron transfer mechanism in diverse Gram-positive bacteria. Nature 562:140–144.
24. Wang D, Kijkla P, Mohamed ME, Saleh MA, Kumseranee S, Punpruk S, Gu T. 2021. Aggressive corrosion of carbon steel by *Desulfovibrio ferrophilus* IS5 biofilm was further accelerated by riboflavin. Bioelectrochemistry 142:107920.
25. Yi Y, Zhao T, Zang Y, Xie B, Liu H. 2021. Different mechanisms for riboflavin to improve the outward and inward extracellular electron transfer of *Shewanella loihica*. Electrochemistry Communications 124:106966.
26. Huang L, Chang W, Zhang D, Huang Y, Li Z, Lou Y, Qian H, Jiang C, Li X, Mol A. 2022. Acceleration of corrosion of 304 stainless steel by outward extracellular electron transfer of *Pseudomonas aeruginosa* biofilm. Corrosion Science 199:110159.
27. Yang Y, Zhou E, Li L, Peng X, Huang Y, Jiang C, Gu T, Wang F, Xu D. 2025. The role of phenazines in marine *Pseudomonas aeruginosa* microbiologically influenced corrosion against 316L stainless steel. Corrosion Science 242:112587.
28. Huang L, Huang Y, Lou Y, Qian H, Xu D, Ma L, Jiang C, Zhang D. 2020. Pyocyanin-modifying genes *phzM* and *phzS* regulated the extracellular electron transfer in microbiologically-influenced corrosion of X80 carbon steel by *Pseudomonas aeruginosa*. Corrosion Science 164:108355.
29. Zhou E, Zhang M, Huang Y, Li H, Wang J, Jiang G, Jiang C, Xu D, Wang Q, Wang F. 2022. Accelerated biocorrosion of stainless steel in marine water via extracellular electron transfer encoding gene phzH of *Pseudomonas aeruginosa*. Water Research 220:118634.

30. Huang Y, Zhou E, Jiang C, Jia R, Liu S, Xu D, Gu T, Wang F. 2018. Endogenous phenazine-1-carboxamide encoding gene *PhzH* regulated the extracellular electron transfer in biocorrosion of stainless steel by marine *Pseudomonas aeruginosa*. Electrochemistry Communications 94:9–13.
31. Price-Whelan A, Dietrich LEP, Newman DK. 2006. Rethinking "secondary" metabolism: physiological roles for phenazine antibiotics. Nat Chem Biol 2:71–78.
32. Price-Whelan A, Dietrich LEP, Newman DK. 2007. Pyocyanin Alters Redox Homeostasis and Carbon Flux through Central Metabolic Pathways in Pseudomonas aeruginosa PA14. Journal of Bacteriology 189:6372–6381.
33. Wang J, Xiong F, Liu H, Zhang T, Li Y, Li C, Xia W, Wang H, Liu H. 2019. Study of the corrosion behavior of *Aspergillus niger* on 7075-T6 aluminum alloy in a high salinity environment. Bioelectrochemistry 129:10–17.
34. Jirón-Lazos U, Corvo F, De la Rosa SC, García-Ochoa EM, Bastidas DM, Bastidas JM. 2018. Localized corrosion of aluminum alloy 6061 in the presence of *Aspergillus niger*. International Biodeterioration & Biodegradation 133:17–25.
35. Dai X, Wang H, Ju L-K, Cheng G, Cong H, Newby BZ. 2016. Corrosion of aluminum alloy 2024 caused by *Aspergillus niger*. International Biodeterioration & Biodegradation 115:1–10.
36. Onan M, Ilhan-Sungur E, Güngör ND, Cansever N. 2018. Biocides Effect on the Microbiologically Influenced Corrosion of Pure Copper by Desulfovibrio sp. J Electrochem Sci Technol 9:44–50.
37. Pu Y, Dou W, Gu T, Tang S, Han X, Chen S. 2020. Microbiologically influenced corrosion of Cu by nitrate reducing marine bacterium *Pseudomonas aeruginosa*. Journal of Materials Science & Technology 47:10–19.
38. Chen Z, Dou W, Chen S, Pu Y, Xu Z. 2022. Influence of nutrition on Cu corrosion by *Desulfovibrio vulgaris* in anaerobic environment. Bioelectrochemistry 144:108040.
39. Pu Y, Tian Y, Hou S, Dou W, Chen S. 2023. Carbon starvation considerably accelerated nickel corrosion by *Desulfovibrio vulgaris*. Bioelectrochemistry 153:108453.
40. Pu Y, Tian Y, Hou S, Dou W, Chen S. 2023. Enhancement of exogenous riboflavin on microbiologically influenced corrosion of nickel by electroactive Desulfovibrio vulgaris biofilm. npj Mater Degrad 7:1–16.
41. San NO, Nazır H, Dönmez G. 2014. Microbially influenced corrosion and inhibition of nickel–zinc and nickel–copper coatings by *Pseudomonas aeruginosa*. Corrosion Science 79:177–183.
42. Michalska J, Sowa M, Socha RP, Simka W, Cwalina B. 2017. The influence of *Desulfovibrio desulfuricans* bacteria on a Ni-Ti alloy: electrochemical behavior and surface analysis. Electrochimica Acta 249:135–144.
43. Liu D, Yang H, Li J, Li J, Dong Y, Yang C, Jin Y, Yassir L, Li Z, Hernandez D, Xu D, Wang F, Smith JA. 2021. Electron transfer mediator PCN secreted by aerobic marine *Pseudomonas aeruginosa* accelerates microbiologically influenced corrosion of TC4 titanium alloy. Journal of Materials Science & Technology 79:101–108.
44. Saleem Khan M, Li Z, Yang K, Xu D, Yang C, Liu D, Lekbach Y, Zhou E, Kalnaowakul P. 2019. Microbiologically influenced corrosion of titanium caused by aerobic marine bacterium *Pseudomonas aeruginosa*. Journal of Materials Science & Technology 35:216–222.

45. Purchase D, Abbasi G, Bisschop L, Chatterjee D, Ekberg C, Ermolin M, Fedotov P, Garelick H, Isimekhai K, Kandile NG, Lundström M, Matharu A, Miller BW, Pineda A, Popoola OE, Retegan T, Ruedel H, Serpe A, Sheva Y, Surati KR, Walsh F, Wilson BP, Wong MH. 2020. Global occurrence, chemical properties, and ecological impacts of e-wastes (IUPAC Technical Report). Pure and Applied Chemistry 92:1733–1767.
46. Jain M, Kumar D, Chaudhary J, Kumar S, Sharma S, Singh Verma A. 2023. Review on E-waste management and its impact on the environment and society. Waste Management Bulletin 1:34–44.
47. Han W, Gao G, Geng J, Li Y, Wang Y. 2018. Ecological and health risks assessment and spatial distribution of residual heavy metals in the soil of an e-waste circular economy park in Tianjin, China. Chemosphere 197:325–335.
48. Bilal M, Guo S, Iqbal HMN, Hu H, Wang W, Zhang X. 2017. Engineering Pseudomonas for phenazine biosynthesis, regulation, and biotechnological applications: a review. World J Microbiol Biotechnol 33:1–11.
49. Maddula VSRK, Pierson EA, Pierson LS. 2008. Altering the Ratio of Phenazines in Pseudomonas chlororaphis (aureofaciens) Strain 30-84: Effects on Biofilm Formation and Pathogen Inhibition. Journal of Bacteriology 190:2759–2766.
50. Kluyver AJ. 1956. *PSEUDOMONAS AUREOFACIENS* NOV. SPEC. AND ITS PIGMENTS. J Bacteriol 72:406–411.
51. Harris DC. 2010. Quantitative Chemical Analysis, 8th ed. W. H. Freeman and Company.
52. Wang Y, Newman DK. 2008. Redox Reactions of Phenazine Antibiotics with Ferric (Hydr)oxides and Molecular Oxygen. Environ Sci Technol 42:2380–2386.
53. Franco A, Elbahnasy M, Rosenbaum MA. 2023. Screening of natural phenazine producers for electroactivity in bioelectrochemical systems. Microbial Biotechnology 16:579–594.
54. Biessy A, Filion M. 2018. Phenazines in plant-beneficial Pseudomonas spp.: biosynthesis, regulation, function and genomics. Environmental Microbiology 20:3905–3917.
55. Siunova TV, Kochetkov VV, Validov SZ, Suzina NE, Boronin AM. 2002. The Production of Phenazine Antibiotics by the Pseudomonas aureofaciens Strain with Plasmid-Controlled Resistance to Cobalt and Nickel. Microbiology 71:670–676.
56. Barras F, Fontecave M. 2011. Cobalt stress in Escherichia coli and Salmonella enterica: molecular bases for toxicity and resistance†. Metallomics 3:1130–1134.
57. Dulay H, Tabares M, Kashefi K, Reguera G. 2020. Cobalt Resistance via Detoxification and Mineralization in the Iron-Reducing Bacterium Geobacter sulfurreducens. Front Microbiol 11.
58. Chen B-Y, Wu C-H, Chang J-S. 2006. An assessment of the toxicity of metals to *Pseudomonas aeruginosa* PU21 (Rip64). Bioresource Technology 97:1880–1886.
59. Greenwood NN, Earnshaw A. 2012. Chemistry of the Elements, 2nd ed. Elsevier Butterworth-Heinemann.
60. Bürstel I, Siebert E, Frielingsdorf S, Zebger I, Friedrich B, Lenz O. 2016. CO synthesized from the central one-carbon pool as source for the iron carbonyl in O2-tolerant [NiFe]-hydrogenase. Proceedings of the National Academy of Sciences 113:14722–14726.

61. De Rosa E, Checchetto V, Franchin C, Bergantino E, Berto P, Szabò I, Giacometti GM, Arrigoni G, Costantini P. 2015. [NiFe]-hydrogenase is essential for cyanobacterium Synechocystis sp. PCC 6803 aerobic growth in the dark. Sci Rep 5:12424.
62. Vignais PM, Billoud B, Meyer J. 2001. Classification and phylogeny of hydrogenases1. FEMS Microbiology Reviews 25:455–501.
63. Coppi MV, O'Neil RA, Lovley DR. 2004. Identification of an Uptake Hydrogenase Required for Hydrogen-Dependent Reduction of Fe(III) and Other Electron Acceptors by Geobacter sulfurreducens. Journal of Bacteriology 186:3022–3028.
64. Crespo A, Blanco-Cabra N, Torrents E. 2018. Aerobic Vitamin B12 Biosynthesis Is Essential for Pseudomonas aeruginosa Class II Ribonucleotide Reductase Activity During Planktonic and Biofilm Growth. Frontiers in Microbiology 9.
65. Debussche L, Couder M, Thibaut D, Cameron B, Crouzet J, Blanche F. 1992. Assay, purification, and characterization of cobaltochelatase, a unique complex enzyme catalyzing cobalt insertion in hydrogenobyrinic acid a,c-diamide during coenzyme B12 biosynthesis in Pseudomonas denitrificans. Journal of Bacteriology 174:7445–7451.
66. Shin D, Park J, Jeong J, Kim B. 2015. A biological cyanide production and accumulation system and the recovery of platinum-group metals from spent automotive catalysts by biogenic cyanide. Hydrometallurgy 158:10–18.
67. Faramarzi MA, Mogharabi-Manzari M, Brandl H. 2020. Bioleaching of metals from wastes and low-grade sources by HCN-forming microorganisms. Hydrometallurgy 191:105228.
68. Pourhossein F, Mousavi SM, Beolchini F, Lo Martire M. 2021. Novel green hybrid acidic-cyanide bioleaching applied for high recovery of precious and critical metals from spent light emitting diode lamps. Journal of Cleaner Production 298:126714.
69. Wargo MJ, Szwergold BS, Hogan DA. 2008. Identification of Two Gene Clusters and a Transcriptional Regulator Required for Pseudomonas aeruginosa Glycine Betaine Catabolism. Journal of Bacteriology 190:2690–2699.
70. Wang S, Pearson LA, Mazmouz R, Liu T, Neilan BA. Heterologous Expression and Biochemical Analysis Reveal a Schizokinen-Based Siderophore Pathway in Leptolyngbya (Cyanobacteria). Appl Environ Microbiol 88:e02373-21.
71. Chuljerm H, Deeudom M, Fucharoen S, Mazzacuva F, Hider RC, Srichairatanakool S, Cilibrizzi A. 2020. Characterization of two siderophores produced by *Bacillus megaterium*: A preliminary investigation into their potential as therapeutic agents. Biochimica et Biophysica Acta (BBA) - General Subjects 1864:129670.
72. Wang Q, Liu Q, Ma Y, Zhou L, Zhang Y. 2007. Isolation, sequencing and characterization of cluster genes involved in the biosynthesis and utilization of the siderophore of marine fish pathogen Vibrio alginolyticus. Arch Microbiol 188:433–439.
73. Reydams H, Toledo-Silva B, Mertens K, Piepers S, Vereecke N, Souza FN, Haesebrouck F, De Vliegher S. 2024. Phenotypic and genotypic assessment of iron acquisition in diverse bovine-associated non-aureus staphylococcal strains. Vet Res 55:6.
74. Ghssein G, Ezzeddine Z. 2022. A Review of Pseudomonas aeruginosa Metallophores: Pyoverdine, Pyochelin and Pseudopaline. Biology (Basel) 11:1711.
75. Braud A, Geoffroy V, Hoegy F, Mislin GLA, Schalk IJ. 2010. Presence of the siderophores pyoverdine and pyochelin in the extracellular medium reduces toxic metal

accumulation in Pseudomonas aeruginosa and increases bacterial metal tolerance. Environmental Microbiology Reports 2:419–425.

76. Demange P, Bateman A, Dell A, Abdallah MA. 1988. Structure of azotobactin D, a siderophore of Azotobacter vinelandii strain D (CCM 289). Biochemistry 27:2745–2752.
77. Pollmann K, Kutschke S, Matys S, Raff J, Hlawacek G, Lederer FL. 2018. Bio-recycling of metals: Recycling of technical products using biological applications. Biotechnology Advances 36:1048–1062.
78. Jerez CA. 2017. Biomining of metals: how to access and exploit natural resource sustainably. Microbial Biotechnology 10:1191–1194.
79. Hmelo LR, Borlee BR, Almblad H, Love ME, Randall TE, Tseng BS, Lin C, Irie Y, Storek KM, Yang JJ, Siehnel RJ, Howell PL, Singh PK, Tolker- Nielsen T, Parsek MR, Schweizer HP, Harrison JJ. 2015. Precision-engineering the Pseudomonas aeruginosa genome with two-step allelic exchange. Nature Protocols 10:1820.
80. Ling C, Peabody GL, Salvachúa D, Kim Y-M, Kneucker CM, Calvey CH, Monninger MA, Munoz NM, Poirier BC, Ramirez KJ, St. John PC, Woodworth SP, Magnuson JK, Burnum-Johnson KE, Guss AM, Johnson CW, Beckham GT. 2022. Muconic acid production from glucose and xylose in Pseudomonas putida via evolution and metabolic engineering. Nature Communications 13.
81. Figurski DH, Helinski DR. 1979. Replication of an origin-containing derivative of plasmid RK2 dependent on a plasmid function provided in trans. Proc Natl Acad Sci U S A 76:1648–1652.
82. Liu K, Hu H, Wang W, Zhang X. 2016. Genetic engineering of Pseudomonas chlororaphis GP72 for the enhanced production of 2-Hydroxyphenazine. Microbial Cell Factories 15:131.
83. Blin K, Shaw S, Vader L, Szenei J, Reitz ZL, Augustijn HE, Cediel-Becerra JDD, de Crécy-Lagard V, Koetsier RA, Williams SE, Cruz-Morales P, Wongwas S, Segurado Luchsinger AE, Biermann F, Korenskaia A, Zdouc MM, Meijer D, Terlouw BR, van der Hooft JJJ, Ziemert N, Helfrich EJN, Masschelein J, Corre C, Chevrette MG, van Wezel GP, Medema MH, Weber T. 2025. antiSMASH 8.0: extended gene cluster detection capabilities and analyses of chemistry, enzymology, and regulation. Nucleic Acids Research gkaf334.
84. Shaffer M, Borton MA, McGivern BB, Zayed AA, La Rosa SL, Solden LM, Liu P, Narrowe AB, Rodríguez-Ramos J, Bolduc B, Gazitúa MC, Daly RA, Smith GJ, Vik DR, Pope PB, Sullivan MB, Roux S, Wrighton KC. 2020. DRAM for distilling microbial metabolism to automate the curation of microbiome function. Nucleic Acids Research 48:8883–8900.

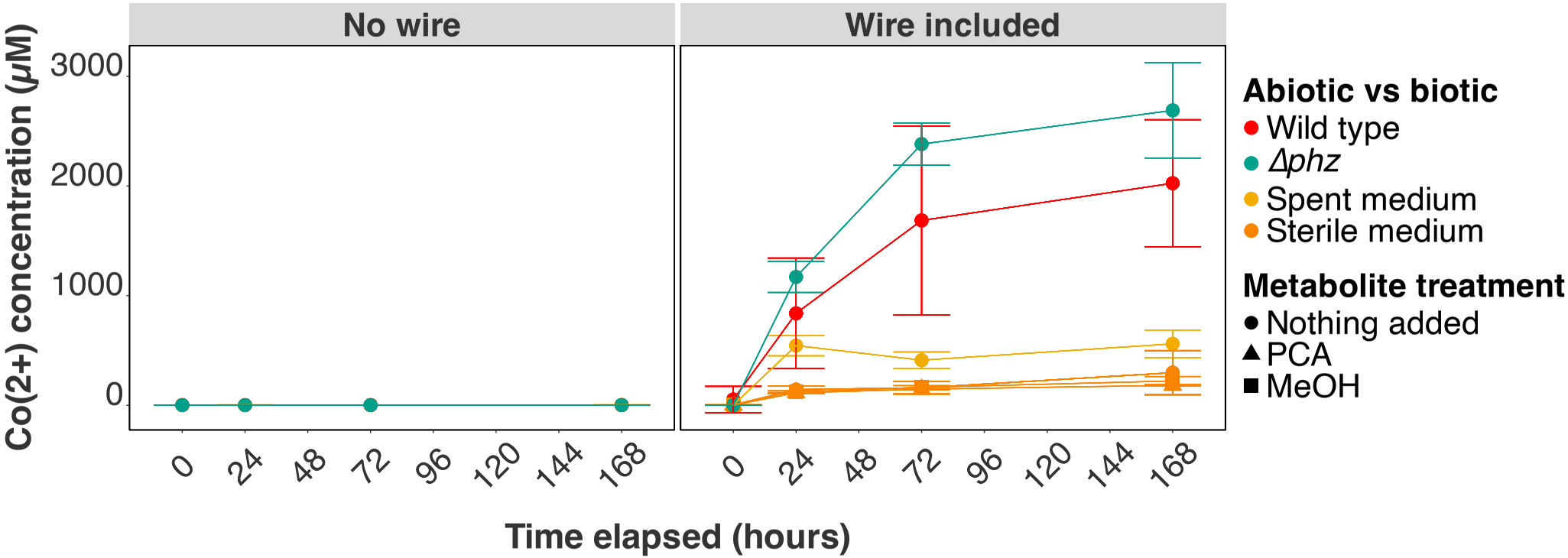
No wire
Wire included
Co(2+) concentration (μM)
3000
2000
1000
0
0
24
48
72
96
120
144
168
Time elapsed (hours)
Abiotic vs biotic
Wild type
Δphz
Spent medium
Sterile medium
Metabolite treatment
Nothing added
PCA
MeOH

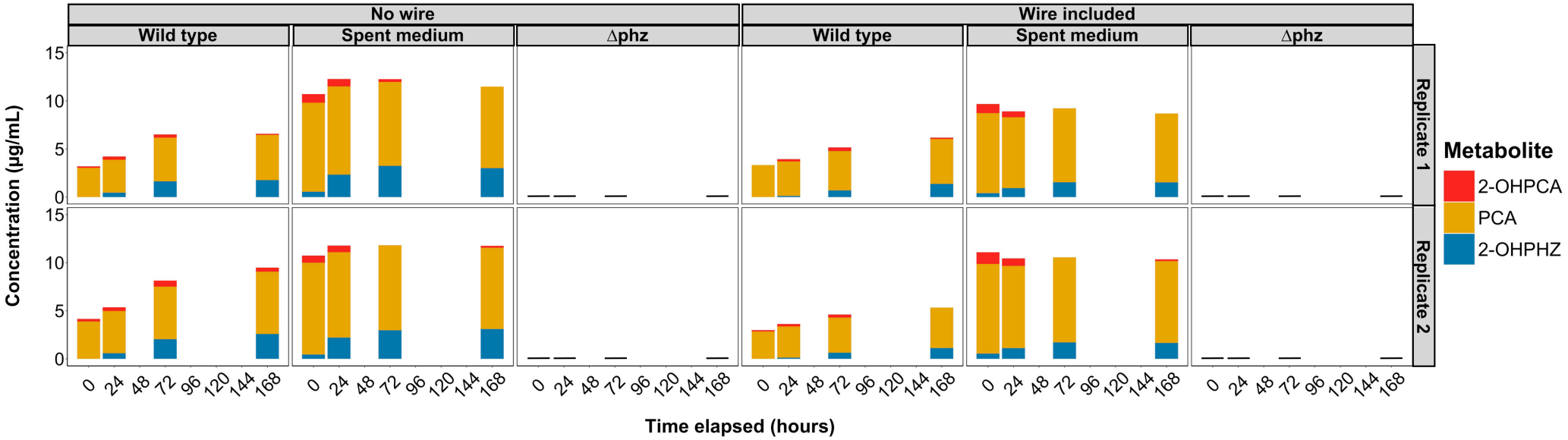
No wire
Wire included
Wild type
Spent medium
Δphz
Wild type
Spent medium
Δphz
Replicate 1
Replicate 2
Concentration (µg/mL)
15
10
5
0
0
24
48
72
96
120
144
168
Time elapsed (hours)
Metabolite
2-OHPCA
PCA
2-OHPHZ

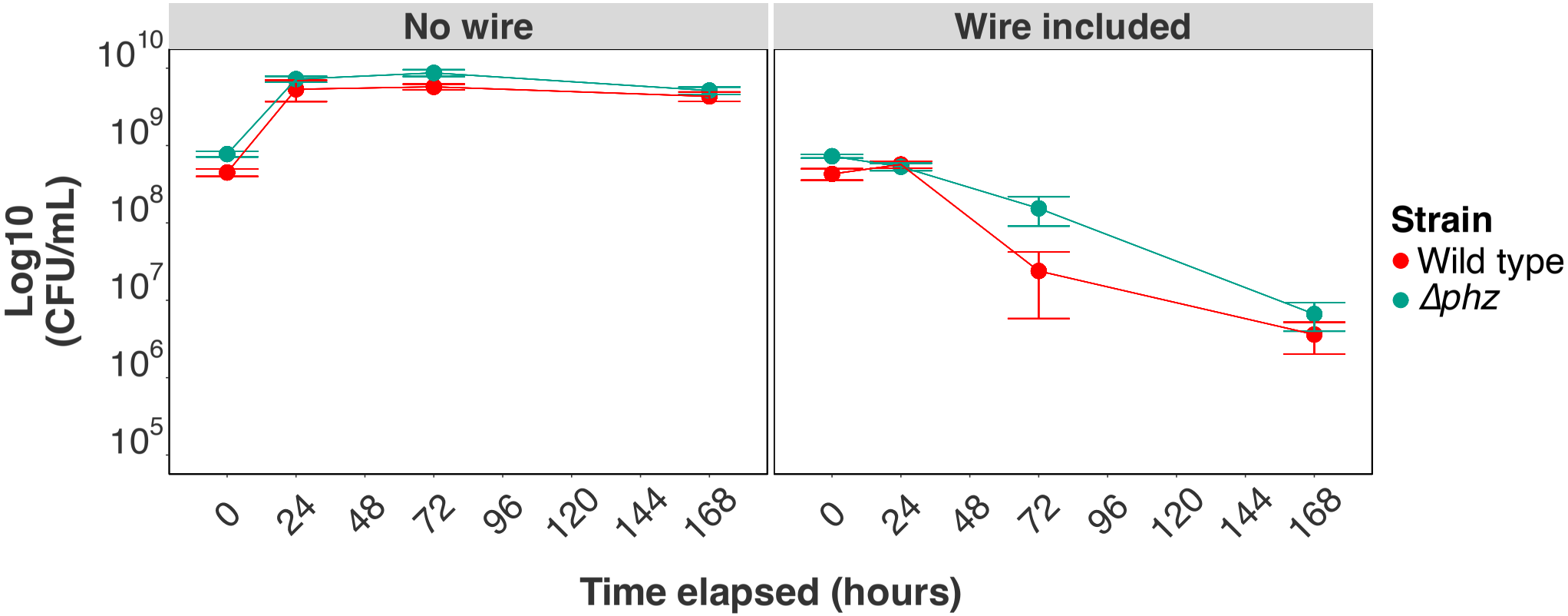
No wire
Wire included
Log10 (CFU/mL)
10^{10}
10^{9}
10^{8}
10^{7}
10^{6}
10^{5}
0
24
48
72
96
120
144
168
Time elapsed (hours)
Strain
Wild type
Δphz

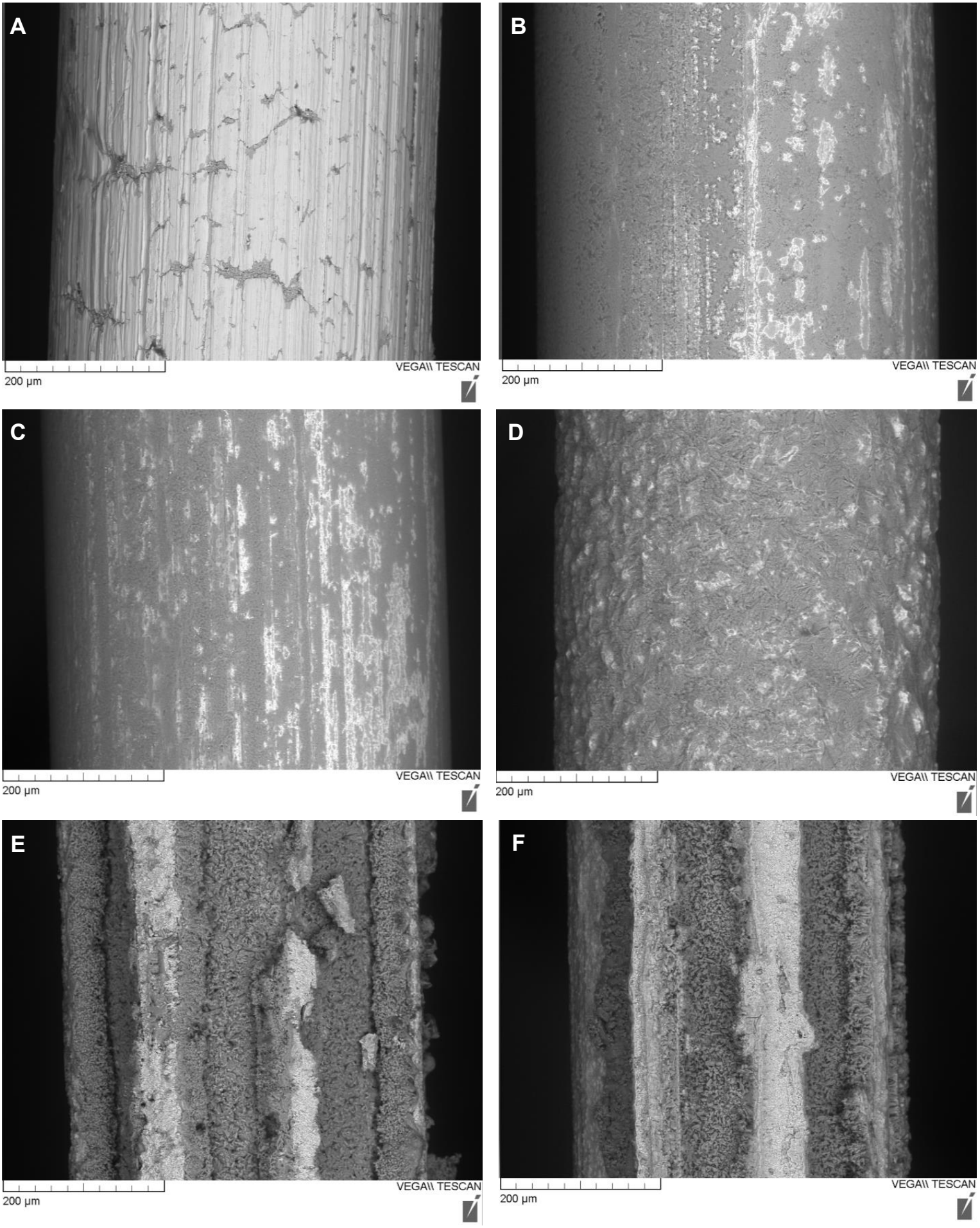
A
200 µm
VEGA\\ TESCAN
B
200 µm
VEGA\\ TESCAN
C
200 µm
VEGA\\ TESCAN
D
200 µm
VEGA\\ TESCAN
E
200 µm
VEGA\\ TESCAN
F
200 µm
VEGA\\ TESCAN

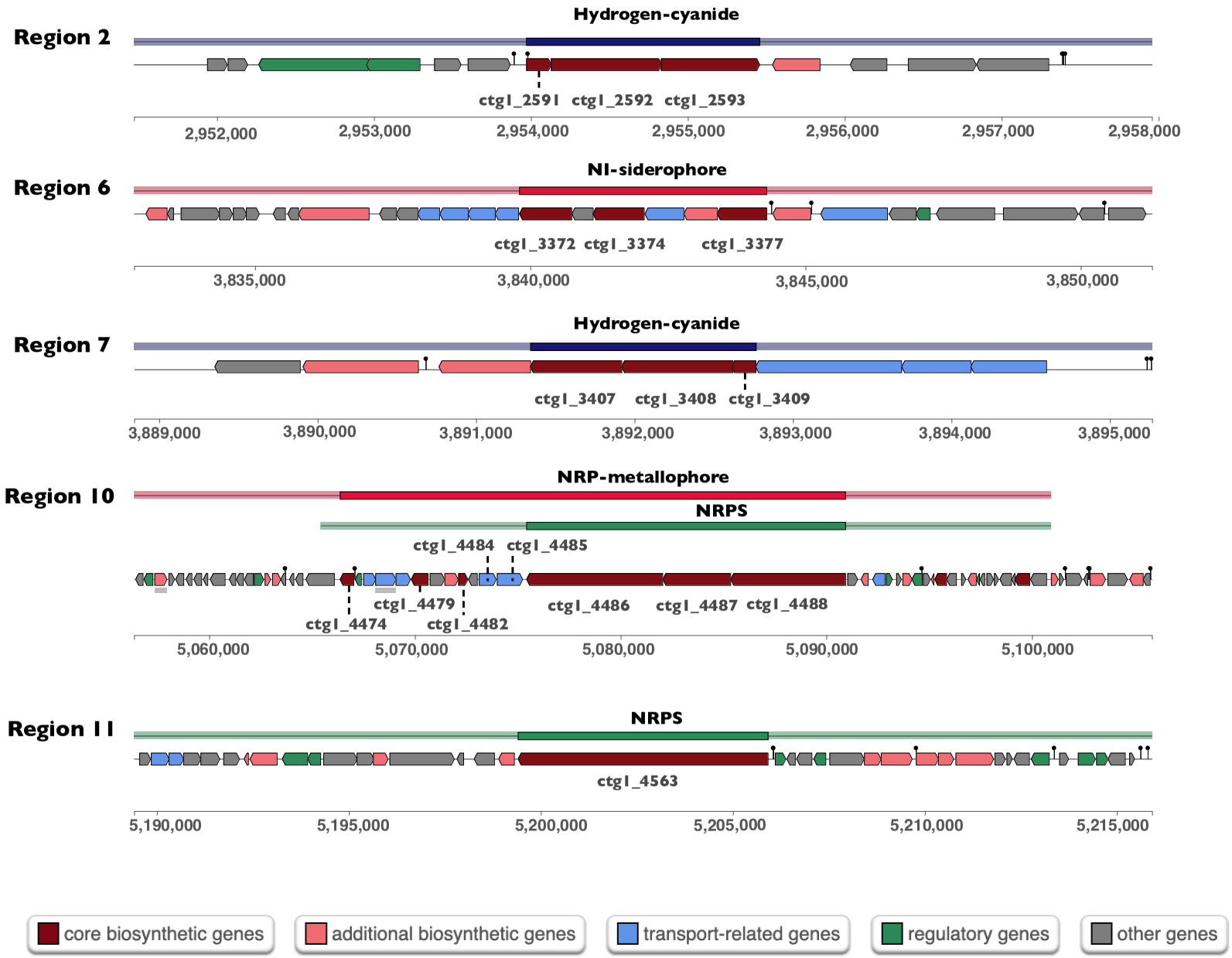
Region 2
Hydrogen-cyanide
ctgl_2591 ctgl_2592 ctgl_2593
2,952,000
2,953,000
2,954,000
2,955,000
2,956,000
2,957,000
2,958,000
Region 6
NI-siderophore
ctgl_3372 ctgl_3374 ctgl_3377
3,835,000
3,840,000
3,845,000
3,850,000
Region 7
Hydrogen-cyanide
ctgl_3407 ctgl_3408 ctgl_3409
3,889,000
3,890,000
3,891,000
3,892,000
3,893,000
3,894,000
3,895,000
Region 10
NRP-metallophore
NRPS
ctgl_4484 ctgl_4485
ctgl_4479
ctgl_4474 ctgl_4482
ctgl_4486 ctgl_4487 ctgl_4488
5,060,000
5,070,000
5,080,000
5,090,000
5,100,000
Region 11
NRPS
ctgl_4563
5,190,000
5,195,000
5,200,000
5,205,000
5,210,000
5,215,000
core biosynthetic genes
additional biosynthetic genes
transport-related genes
regulatory genes
other genes